Am J Transl Res 2025;17(4):3094-3108
www.ajtr.org /ISSN:1943-8141/AJTR0164274

Original Article

H3K9me3 and H3K27me3 are epigenetic barriers to somatic cell nuclear transfer in rabbits

Yuan Gao[1*], Fangfang Wu[1*], Dandan Tang[1], Xiao Chen[1], Qian Chen[2], Ying Chen[1], Kexin Fang[1], Wanxin Chen[1], Fuliang Du[1], Zhihui Liu[1]

[1]Jiangsu Key Laboratory for Molecular and Medical Biotechnology, College of Life Sciences, Nanjing Normal University, Nanjing 210046, Jiangsu, PR China; [2]Changde First Hospital of Traditional Chinese Medicine, Changde Affiliated Hospital, Hunan University of Chinese Medicine, Changde 415000, Hunan, PR China. [*]Equal contributors.

Received March 2, 2025; Accepted April 11, 2025; Epub April 15, 2025; Published April 30, 2025

Abstract: Somatic cell nuclear transfer (NT) is associated with aberrant changes in epigenetic reprogramming that disrupt embryo development. Here, we characterized the epigenetic patterns of histone 3 lysine 9 trimethylation (H3K9me3) and histone 3 lysine 27 trimethylation (H3K27me3), the repressive histone signature in heterochromatin, in NT rabbit embryos. H3K9me3 modification was higher in all stages of NT vs. fertilized preimplantation embryos, consistent with decreased transcription of the H3K9me3 demethylase *KDM3B* in four-cell and eight-cell NT embryos vs. fertilized embryos. H3K27me3 was higher in NT embryos from two-cell stage to the blastocyst, and transcription of the H3K27me3 demethylase *KDM6A* was lower in four-cell and eight-cell NT embryos than in fertilized embryos. Cleavage under targets and tagmentation (CUT and Tag) showed enrichment of whole-chromosome H3K9me3 and H3K27me3 in four-cell and eight-cell NT vs. fertilized embryos. Further, eight-cell NT embryos had a higher proportion of H3K9me3 and H3K27me3 sites around the promoter regions of the genome compared to fertilized embryos. The genes associated with H3K9me3 sites near promoter regions were primarily related to the development of tissues and organs, whereas the H3K27me3 enriched regions mainly influenced the development and regulation of the nervous system. Our findings demonstrate that H3K9me3 and H3K27me3 inhibit the expression of genes essential for the development and preimplantation of NT embryos and, thus, are epigenetic barriers to NT reprogramming in rabbits.

Keywords: Somatic cell nuclear transfer, rabbit embryos, H3K9me3, H3K27me3, epigenetic barrier

Introduction

Somatic cell nuclear transfer (NT) is a technology that efficiently reprograms terminally differentiated somatic cells to a totipotent state, allowing their development into a specified animal species [1]. Since the first cloned mammal, 'Dolly' the sheep, was born in 1997 [2], more than 20 mammalian species have been cloned successfully [3]. However, the cloning efficiency of NT is much lower than *in vitro* fertilization, as described in rabbits [4]. Abnormal methylation, including histone 3 lysine 4 trimethylation (H3K4me3) [5], histone 3 lysine 9 trimethylation (H3K9me3) [6], histone 3 lysine 27 trimethylation (H3K27me3) [7, 8], histone 4 lysine 20 trimethylation (H4K20me3) [9], and DNA hypermethylation [10, 11] as well as developmental defects such as X chromosome inactivation [12] in NT embryos limit cloning success [3].

After mice and rats, rabbits are the third most often used experimental mammal [13, 14], providing unique advantages as transgenic bioreactors and as models for human diseases and human reproduction [4]. The first rabbit was successfully cloned in 2002 using a cumulus cell as the nuclear donor, but the cloning efficiency was only 1.6% [15]. However, several strategies mitigate abnormal epigenetic modifications and improve the efficiency of NT reprogramming in rabbits. 1) Sperm-borne small RNAs miR-34c and miR-125b that decrease levels of H3K9me3 improve the developmental competence of rabbit NT embryos [16]. 2)

https://doi.org/10.62347/FQYG9348

Sperm-borne proteins improve rabbit NT efficiency by regulating embryonic cleavage and epigenetics [17]. 3) Melatonin protects rabbit NT embryos from electrofusion damage [18]. We demonstrated previously that young oocytes improve rabbit NT [19], follicular oocytes support rabbit NT development better than oviductal oocytes [20], and trichostatin A and scriptaid synergistically improve rabbit NT embryo development [21].

Histone methylation, depending on its location, either activates or represses transcription. H3K4me3, H3K36me3, and H3K79me3 are associated with activation of transcription, whereas H3K9me3, H3K27me3, and H4K20me3 are associated with repression of transcription [22]. H3K9me3, a hallmark of heterochromatin that is typically located in the promoters of repressed genes, is required for constitutive heterochromatin formation in pericentromeric and centromeric DNA [23]. H3K9me3 modification is dynamically regulated by SUV39H1/2, a homolog of the KDM4 histone demethylase [6]. H3K9me3 is a major epigenetic barrier in mouse, human, pig, and bovine NT embryos [6, 24-26]. H3K27me3, which also represses transcription, is methylated by enhancer of zeste homolog (EZH)2 [27] and demethylated by KDM6A and KDM6B [28]. Although aberrant H3K27me3 occurs in mouse, pig, and bovine NT embryos [7, 8, 29], the role and regulation mechanism of H3K9me3 and H3K27me3 in rabbit NT embryos during reprogramming are unclear.

Here, we characterized the dynamic aberrant patterns of H3K9me3 and H3K27me3 in cloned preimplantation rabbit embryos and the factors that regulate H3K9me3 and H3K27me3 during NT reprogramming, including the histone demethylase gene *KDM3B* for H3K9me3 and *KDM6A* for H3K9me3. Additionally, we compared and analyzed the cleavage under targets and tagmentation (CUT and Tag) data for NT four-cell to eight-cell zygotic genome activation (ZGA) embryos and showed that H3K9me3 and H3K27me3 disrupted gene expression, especially developmental genes, during rabbit NT reprogramming. We demonstrated that aberrant H3K9me3 and H3K27me3 modifications in cloned rabbit embryos act as molecular regulators and epigenetic barriers to nuclear reprogramming.

Materials and methods

Chemicals and reagents

Unless otherwise stated, all chemicals were obtained from MilliporeSigma (St. Louis, MO, USA). All animal care and use procedures were approved by the Animal Care and Use Committee of Nanjing Normal University (IACUC-20230230) and performed according to the United States National Institutes of Health guidelines.

Animal maintenance, hormone-induced superovulation, oocytes, and in vivo fertilized embryos

Sexually mature (6-12-month-old) New Zealand White (NZW) rabbits that purchased from Nanjing rabbit farm were maintained under a 12-h dark/light cycle. Female donors were superovulated as described previously [30] by administering follicle-stimulating hormone (FSH, NSHF, Ningbo Second Hormone Factory, Ningbo, China) (33 IU/mL) in two 0.3-mL, two 0.4-mL, and two 0.5-mL doses at 12-h intervals, followed by 150 IU of human choriogonadotropin (hCG) (NSHF, Ningbo, China). The method of ear intravenous injection of 30 ml air was used to perform the euthanasia. We collected oocytes and cumulus for NT from the oviduct of the donor NZW rabbit, not mated with males, 11 h after hCG injection using Dulbecco's phosphate-buffered saline (DPBS, 14190-144, Gibco, Grand Island, NY). To obtain fertilized embryos, after the hCG injection, female NZW rabbits were mated with males to establish pregnancies. After 18 h, 28 h, 38 h, 48 h, 84 h, and 106 h, the one-cell, two-cell, four-cell, eight-cell, morula, and blastocyst embryos were flushed with DPBS plus 0.1% polyvinyl alcohol (PVA) and cultured in 2.5% fetal bovine serum (FBS) (HyClone, USA) B2 medium (Laboratories CCD, France) at 38.5°C in 5% CO_2 and humidified air prior to embryo seeding.

Donor cell preparation, nuclear transfer, and NT embryo culture

Freshly harvested cumulus cells, prepared as described previously [20], served as the NT nuclear donors. Briefly, we digested cumulus and oocyte compacts, flushed from the oviduct 11 h after FSH injection, with 0.1% hyaluronidase (H3506) to collect the cumulus cells. They

were washed in Ca^{2+}- and Mg^{2+}- free DPBS supplemented with 10% polyvinylpyrrolidone (PVP-40) and centrifuged at 1000×g. The cells were digested in trypsin-ethylene diamine tetra acetic acid at 37°C for 3 min, then suspended in 10% FBS DMEM (Gibco) and maintained at 37°C prior to NT.

As described previously [20], we used a glass needle to enucleate rabbit oocytes by cutting the zona pellucida and applying pressure to extrude the polar body and adjacent cytoplasm (1/16 of the total cytoplasm). We stained the samples with 10 μg/mL Hoechst 33342 dye to demonstrate the loss of the nucleus by fluorescence microscopy. We transferred a 13-15 μm donor cumulus cell into the perivitelline space of an enucleated rabbit oocyte and incubated the pair in a fusion medium (0.3 M mannitol supplemented with 0.1 mM $CaCl_2$ and 0.1 mM $MgCl_2$) for 1 min. To induce cell fusion, we applied three direct current (DC) pulses of 3.2 kV/cm for a duration of 20 μs /each using a BTX 200 Electro Cell Manipulator (Biotechnologies and Experimental Research Inc., San Diego, CA) to the cells that had been placed in an electrical chamber with wires at 1 mm apart in the fusion medium. NT oocytes were then incubated for 90 min in M199 medium at 38.5°C.

The fused NT embryos were activated by treating them with the same electrical DC charge used for cell fusion, followed by a 1 h incubation in M199 + 10% FBS containing 2.0 mM 6-dimethylaminopurine (D2629) and 5 μg/mL cycloheximide (C6255). After activation, the NT embryos were subjected to *in vitro* culture (IVC) in B2 medium at 38.5°C under 5% CO_2 in a humidified atmosphere. One-cell, two-cell, four-cell, eight-cell, morula, and blastocyst NT embryos were collected after 12 h, 18 h, 26 h, 36 h, 72 h, and 102 h IVC, respectively.

Immunofluorescence staining, microscopy, and image analysis

Fertilized and NT rabbit embryos were fixed with fresh 4% paraformaldehyde for 10 min at room temperature (RT), washed, and stored in DPBS at 4°C. Embryos were permeabilized with 0.5% Triton-X 100 (Beyotime, China) for 20 min and washed three times at RT, followed by blocking with DPBS containing 2% FBS for 1 h at RT. The samples were treated with a primary monoclonal antibody against H3K9me3 (CST, Cat. 5327T, dilution 1:100) or H3K27me3 (Abcam, Cat. Ab6002, dilution 1:200) overnight at 4°C. After washing for 10 min in DPBS, we treated samples with the secondary antibody Alexa Fluor 488 IgG (Fcmacs, Nanjing, China, Cat. Msaf48801, dilution 1:200) in the dark for 1 h at RT. We stained the embryos with 4,6-diamidino-2-phenylindole (DAPI; 100 ng/ml; D9564) for 10 min, mounted them on slides, and collected 500 ms fluorescent images (Olympus BX53, Japan). We calculated the fluorescence intensity as the nuclear area times the average optical density per unit area of an embryo using ImageJ (v1.8.0; National Institutes of Health) as described previously [9]. We changed the images to 16-bit greyscale and used the background subtract function before we measured and compared the intensities of the nuclear regions in the images for the NT and fertilized embryos.

Cleavage under targets and tagmentation (CUT and Tag) assay

The CUT and Tag assay was performed using the Hyperactive Universal CUT and Tag Assay Kit for Illumina Pro (Vazyme Biotech, #TD904), as described previously [31]. Briefly, after activating the concanavalin A beads, 100 μl of wash buffer was added to the samples of fertilized and NT rabbit embryos (5 four-cell and 3 eight-cell embryos for one batch) and incubated on a rotator at RT for ten min. Embryos were then incubated overnight at 4°C with the H3K9me3 and H3K27me3 antibody-bead complex on a rotator. Following incubation with the secondary antibody, the samples were mixed with pA/G-Tnp and incubated on a rotator for 1 h. The samples were then tagmented in 40 μl of tagmentation buffer at 37°C for 1 h. following the manufacturer's instructions, DNA was extracted and dissolved in 20 μl of nuclease-free water. To amplify the libraries, we added P5/P7 primers (Vazyme Biotech, #TD202) and 2× CAM (CUT and Tag Amplification Mix) and performed polymerase chain reaction (PCR). The DNA was cleaned using two volumes of DNA cleaning beads (Vazyme Biotech, #N411), and the libraries were eluted in 20 μl of nuclease-free water. The samples were pooled and sequenced using 150 bp paired-end reads on the Illumina NovaSeq 6000 platform.

CUT and Tag data processing

The CUT and Tag data processing and analysis were done essentially as we described previously [31]. Sequencing adapters were trimmed,

Table 1. Sequences of primers for reverse transcription-quantitative polymerase chain reaction (RT-qPCR)

Gene Symbol	Forward Primer (5'-3')	Reverse Primer (5'-3')
SUV39H1	GCTTCCGCACCCATAAGATGA	AGGTCCCGTTGCCTTAGGA
SUV39H2	ACCTTCAAGATCGACATCGACC	ACTTCTGACCTGCTACCGGAA
KDM3B	ACCTATGCGGACAATTCATC	CAGACCAGAGACTGGGATAC
KDM4B	AGATTGAAGCCCTCAAAGG	AGCTTGACGTTCATAAGCTC
EZH2	CTGAGCGGATAAAGACCCCC	ATCACACAAGGGCACGAACT
KDM6A	CCACCCTGCCTAGCAATTCA	TCCTCCATCCCTTCTCCGTT
KDM6B	GAGCGGTGTTTGTGTTGGAA	TTCCCCAAGGTCTCCCAGG
HPTR1	ACGTCGAGGACTTGGAAAGGGTGTT	GGCCTCCCATCTCCTTCATCACATC

and read pairs with low quality or low complexity were filtered out using TrimGalore (v0.6.10). We then aligned the high-quality read pairs with the reference genome using Bowtie 2 (v2.5.2) with default parameters, retaining only alignments with the best mapping quality [32]. For the alignment, we used the Ensembl OryCun2.0 rabbit reference transcriptome along with a gene transfer format (GTF) file that includes additional coding sequences and exon entries [33]. Duplicate reads were removed using Sambamba (v1.0) [34]. Alignments with low mapping quality and multiple-mapping reads were filtered out using SAMtools (v1.20) [35]. Peaks were called using MACS2 (v2.2.9.1) [36] with the following arguments: "-p 0.05 -broad -broad-cutoff 0.05 -g hs/mm -f BAMPE" for broad peaks. To reduce background noise, we identified highly reproducible peaks using the IDR package [37]. Finally, we used deepTools (v3.5.5) to visualize histone modification signals or genes [38]. We used the "annotatePeak" function in R package ChIPseeker (v1.36.0) to profile the distribution of genomic regions [39, 40].

Annotation and enrichment analysis of genomic regions

We used the "annotatePeak" function in the R package ChIPseeker (v1.36.0) to profile the distribution of genomic regions. We used the R package clusterProfiler (v4.8.3) [41] to perform functional enrichment analysis, also known as Gene Ontology analysis.

Reverse transcription-quantitative polymerase chain reaction (RT-qPCR)

Separate pools of 15 four-cell embryos or 10 eight-cell NT or fertilized rabbit embryos were lysed in 50 μl lysing buffer (Cat. G916, Abm, USA) at 37°C for 15 min, and 5 μl of stop buffer (Abm) was added to stop the reaction and release the RNA. cDNA was synthesized by reverse transcription using 5× All-in-One RT MasterMix (Abm) followed by a 10 min incubation at 25°C, 30 min at 42°C, and 5 min at 85°C according to the manufacturer's instructions. The gene encoding β-actin was used to normalize transcripts. Primers are shown in **Table 1**. RT-qPCR was carried out using the EvaGreen 2× qPCR MasterMix-ROX system (Abm), and the relative mRNA level was calculated as described previously [42, 43].

Data access

The raw sequence data reported in this paper have been deposited in the Genome Sequence Archive [44] in National Genomics Data Center [45], China National Center for Bioinformation/Beijing Institute of Genomics, Chinese Academy of Sciences (GSA: CRA020041) that are publicly accessible at https://ngdc.cncb.ac.cn/gsa/s/hn6cp3Sl.

Statistical analysis

One-way ANOVA was used to evaluate the differences in H3K9me3 and H3K27me3 fluorescence intensity for NT and fertilized embryos at different stages of development. Data on RT-qPCR were analyzed using SPSS 18.0 (IBM, Chicago, IL, USA). Comparisons between two groups were made by Student's two-t ailed t tests. Statistical significance was defined as $P < 0.05$.

Results

Patterns of H3K9me3 and expression of methyltransferase and demethylase RNA in fertilized and NT rabbit embryos

Preimplantation rabbit embryos (one-cell, two-cell, four-cell, eight-cell, morula, and blastocyst)

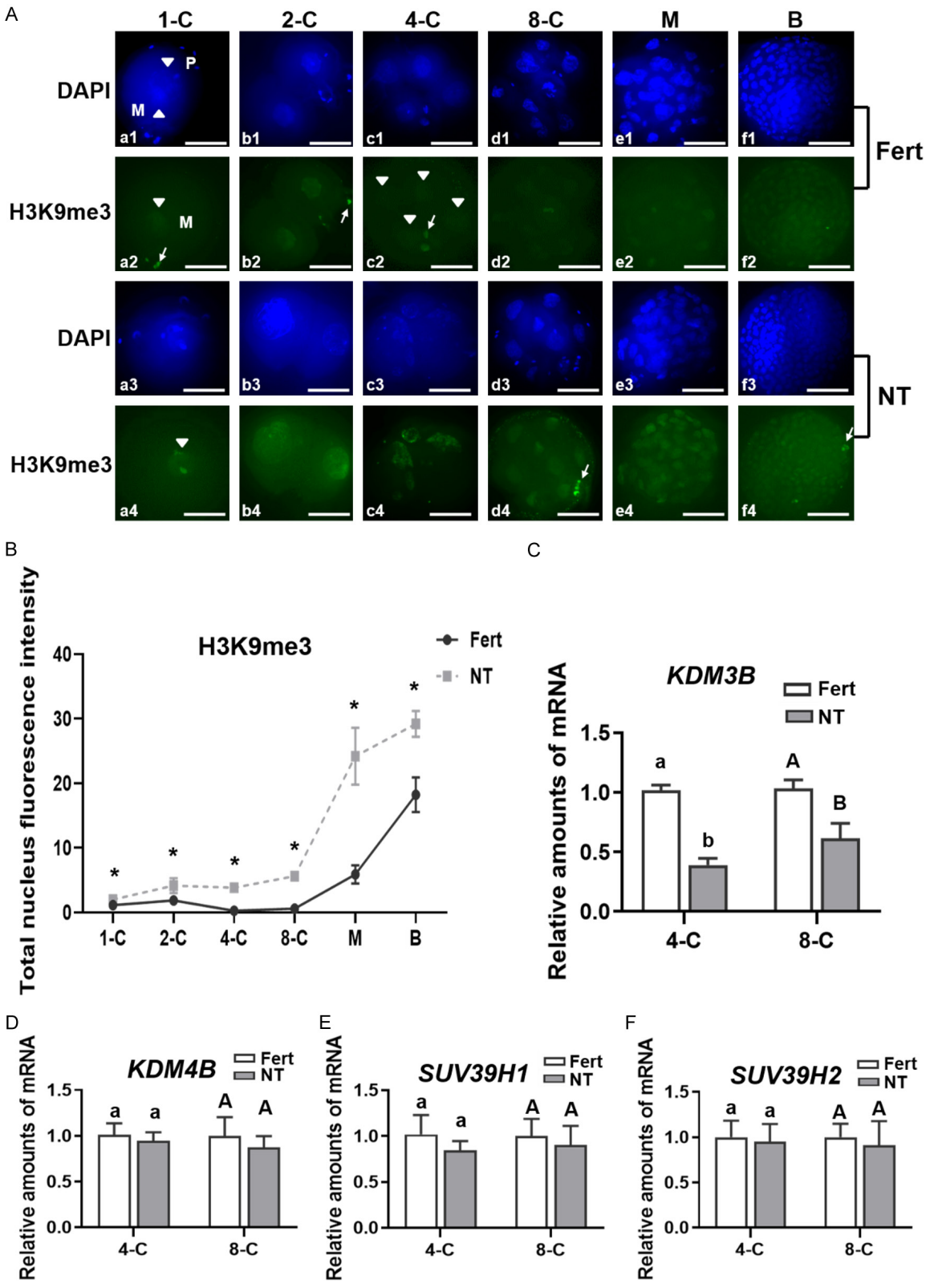

Figure 1. Patterns of H3K9me3 and expression of methyltransferase and demethylase RNA in fertilized and NT rabbit embryos. (A) H3K9me3 immunofluorescence staining increased in one-cell, two-cell, four-cell, eight-cell, morula, and blastocyst NT embryos compared to fertilized embryos. Arrows indicate the H3K9me3 signal in polar bodies, and arrowheads indicate weak H3K9me3 staining. M, maternal nuclear; P, paternal nuclear; Fert, fertilization. NT,

somatic cell nuclear transfer. Scale bar = 70 μm. (B) H3K9me3 immunofluorescence staining of two-cell, four-cell, eight-cell, and morula NT embryos vs. fertilized embryos. *$P < 0.05$. RNA expression levels of (C) demethylase *KDM3B and* (D) *KDM4B,* (E) histone methyltransferases (HMT) *SUV39H1* and (F) *SUV39H2* in four-cell and eight-cell rabbit NT and fertilized embryos. Different lower-case letters (a, b) and upper-case letters (A, B) for four-cell and eight-cell embryos, respectively, in (C) indicate $P < 0.05$. There was no significant difference in *KDM4B* and *Suv39h1/2* RNA expression between NT and fertilized embryos. Experiments were done in triplicate with a total of 190 fertilized embryos (115 embryos for immunofluorescence staining, and 75 for RT-qPCR) and 187 NT embryos (112 for immunofluorescence staining, and 75 for RT-qPCR).

derived by *in vivo* fertilization (without IVC as controls) or NT showed different patterns of H3K9me3. After fertilization, one-cell maternal nuclei showed weak H3K9me3 fluorescence that persisted in the two-cell, four-cell, eight-cell stages, morula, and blastocyst stages. NT embryos had a greater H3K9me3 fluorescence from the two-cell to blastocyst stages than the fertilized controls (**Figure 1A**). H3K9me3 fluorescence intensity was higher in one-cell (2.0, n = 22), two-cell (4.1, n = 21), four-cell (3.9, n = 20), eight-cell (5.7, n = 16), morula (24.2, n = 15), and blastocyst (29.2, n = 15) NT embryos than in fertilized embryos (one-cell, 1.1, n = 18; two-cell, 1.9, n = 20; four-cell, 0.3, n = 21; eight-cell, 0.6, n = 20; morula, 5.9, n = 18; blastocyst, 18.3, n = 15) (**Figure 1B**).

To determine why NT embryos had higher H3K9me3 signals than fertilized embryos, we measured the RNA expression of histone methyltransferase (HMT) genes *SUV39H1/2* and demethylase genes *KDM3B* and *KDM4B* in the ZGA four-cell and eight-cell stages of NT and fertilized embryos by RT-qPCR. Four-cell and eight-cell fertilized embryos had more *KDM3A* RNA than NT embryos (**Figure 1C**, $P < 0.05$), whereas *KDM4B*, *SUV39H1*, and *SUV39H2* were expressed similarly in NT and fertilized embryos (**Figure 1D**, $P > 0.05$).

CUT&Tag analysis of H3K9me3 in fertilized and NT rabbit embryos during ZGA

As H3K9me3 levels were higher in NT embryos than in fertilized embryos, we performed a CUT&Tag analysis on four-cell and eight-cell ZGA NT and fertilized embryos. We found a 1.7-fold increase in H3K9me3 peaks in NT vs. fertilized four-cell embryos (29842 vs. 17899 peaks, respectively) and a 3-fold increase in NT vs. fertilized eight-cell embryos (43380 vs 14254 peaks, respectively) (**Figure 2A**). The percentage of H3K9me3 sites localized to promoter regions (mainly < 1 kb from the transcription starts site [TSS]), was higher in NT (16.1%) vs. fertilized (14.5%) four-cell embryos and in NT (10.6%) vs. fertilized (6.5%) eight-cell embryos (**Figure 2B**). Additionally, the H3K9me3 signal intensities near TSS and transcription end sites (TES) in NT embryos was higher than in fertilized embryos (**Figure 2C**). Thus, enrichment of H3K9me3 at the TSS contributes to transcriptional repression, disrupting the developmental progression of NT rabbit embryos.

Gene Ontology (GO) analysis indicated that the genes associated with the higher H3K9me3 peaks in NT four-cell embryos affect pathways such as the regulation of neuron projection development, dendrite development, cellular component size, and cell growth, highlighting their roles in neurodevelopment and cellular architecture modulation (**Figure 2D**). In contrast, the genes associated with the higher H3K9me3 peaks in eight-cell NT embryos affect pathways such as dendrite development and neuron projection development (**Figure 2E**). Overall, the genes associated with high H3K9me3 binding are primarily related to the development of tissues and organs.

Patterns of H3K27me3 and expression of methyltransferase and demethylase RNA in fertilized and NT rabbit embryos

H3K27me3 fluorescence was undetectable in fertilized one-cell, two-cell, four-cell, and eight-cell nuclei but was present in morula embryos and was weakly distributed in most blastocyst cells (**Figure 3A**). We found weak H3K27me3 fluorescence in two-cell and four-cell NT embryos, which increased in the eight-cell, morula, and blastocyst stages (**Figure 3A**). Similarly, we found lower H3K27me3 fluorescence in two-cell, four-cell, eight-cell, morula, and blastocyst stages in fertilized embryos compared to NT embryos (**Figure 3B**, $P < 0.05$).

To determine why NT embryos had higher H3K27me3 modification than fertilized embryos, we measured the RNA expression of the

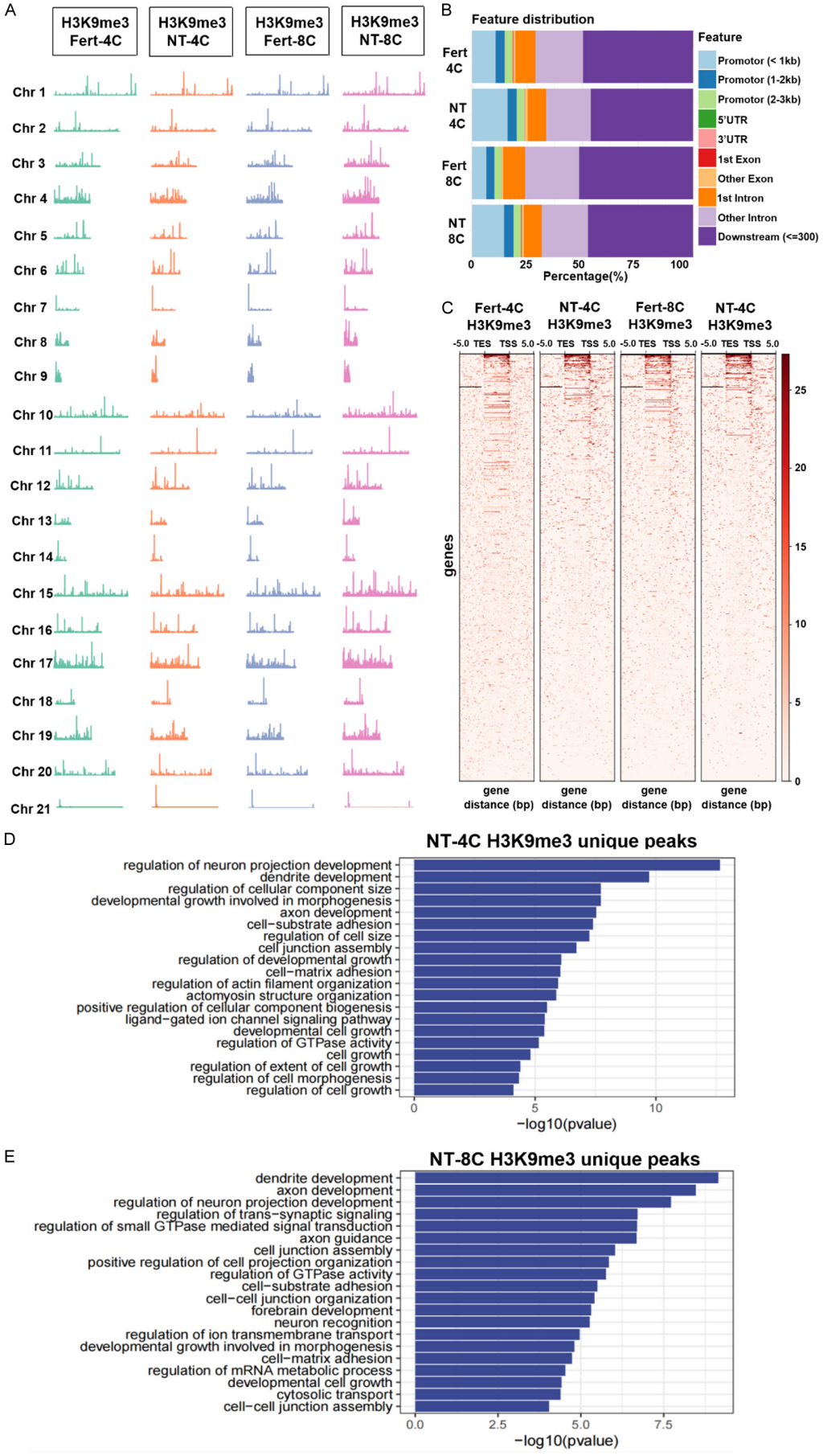
A
H3K9me3 Fert-4C
H3K9me3 NT-4C
H3K9me3 Fert-8C
H3K9me3 NT-8C
Chr 1
Chr 2
Chr 3
Chr 4
Chr 5
Chr 6
Chr 7
Chr 8
Chr 9
Chr 10
Chr 11
Chr 12
Chr 13
Chr 14
Chr 15
Chr 16
Chr 17
Chr 18
Chr 19
Chr 20
Chr 21
B
Feature distribution
Fert 4C
NT 4C
Fert 8C
NT 8C
0
25
50
75
100
Percentage(%)
Feature
Promotor (< 1kb)
Promotor (1-2kb)
Promotor (2-3kb)
5'UTR
3'UTR
1st Exon
Other Exon
1st Intron
Other Intron
Downstream (<=300)
C
Fert-4C H3K9me3
NT-4C H3K9me3
Fert-8C H3K9me3
NT-4C H3K9me3
-5.0 TES TSS 5.0
genes
gene distance (bp)
25
20
15
10
5
0
D
NT-4C H3K9me3 unique peaks
regulation of neuron projection development
dendrite development
regulation of cellular component size
developmental growth involved in morphogenesis
axon development
cell−substrate adhesion
regulation of cell size
cell junction assembly
regulation of developmental growth
cell−matrix adhesion
regulation of actin filament organization
actomyosin structure organization
positive regulation of cellular component biogenesis
ligand−gated ion channel signaling pathway
developmental cell growth
regulation of GTPase activity
cell growth
regulation of extent of cell growth
regulation of cell morphogenesis
regulation of cell growth
0
5
10
−log10(pvalue)
E
NT-8C H3K9me3 unique peaks
dendrite development
axon development
regulation of neuron projection development
regulation of trans−synaptic signaling
regulation of small GTPase mediated signal transduction
axon guidance
cell junction assembly
positive regulation of cell projection organization
regulation of GTPase activity
cell−substrate adhesion
cell−cell junction organization
forebrain development
neuron recognition
regulation of ion transmembrane transport
developmental growth involved in morphogenesis
cell−matrix adhesion
regulation of mRNA metabolic process
developmental cell growth
cytosolic transport
cell−cell junction assembly
0.0
2.5
5.0
7.5
−log10(pvalue)

Figure 2. Global CUT and Tag analysis of H3K9me3 dynamics in NT and fertilized embryos. (A) Distribution of H3K9me3 binding sites across chromosomes (Chr) 1-21 in four-cell and eight-cell fertilized and NT embryos. Each row represents a chromosome, and each colored line represents the signal intensity of the chromatin modification. (B) The stacked bar chart illustrates the distribution of H3K9me3 CUT and Tag peaks on genomic features for four-cell and eight-cell NT vs. fertilized embryos and shows the increase for NT embryos, primarily in promoter regions, particularly < 1 kb from the TSS. (C) A heatmap showing increased H3K9me3 peaks from the TSS to the TES in four-cell and eight-cell NT vs. fertilized embryos. A darker red color indicates higher expression levels. TSS, transcription start site. TES, transcription end site. (D and E) A Gene Ontology (GO) analysis of the H3K9me3 unique peaks in which NT embryos bound more H3K9me3 than fertilized embryos identified primarily genes that affect development. The x-axis, the -log10 (*P*-value), indicates the significance of the enrichment for each GO term. Experiments were done in triplicate with 15 four-cell and -9 eight-cell embryos each for fertilized and NT embryos.

HMT gene *EZH2* and demethylase genes *KDM6A* and *KDM6B* at the four-cell and eight-cell ZGA stages of NT and fertilized embryos by RT-qPCR. Four-cell and eight-cell fertilized embryos had more *KDM6A* RNA than NT embryos (**Figure 3C**, $P > 0.05$), whereas *KDM6B* and *EZH2* were expressed similarly in NT and fertilized embryos (**Figure 3D**, **3E**, $P > 0.05$).

CUT&Tag analysis H3K27me3 in fertilized and NT embryos during ZGA

We performed a CUT&Tag analysis for H3K27me3 on four-cell and eight-cell ZGA NT and fertilized embryos. We found a 2.1-fold increase in H3K27me3 peaks in NT vs. fertilized four-cell embryos (71413 vs. 34413 peaks, respectively) and a 2.9-fold increase in NT vs. fertilized eight-cell embryos (98370 vs 33953 peaks, respectively) (**Figure 4A**). We found that the percentage of H3K27me3 binding sites in promoter regions of four-cell NT embryos (9.6%) was similar to fertilized embryos (9.5%), whereas eight-cell NT embryos had more H3K27me3 peaks in the promoter regions (9.5%) than did fertilized eight-cell embryos (7.3%) (**Figure 4B**). Additionally, the H3K27me3 signal intensities near TSS and TES in four-cell and eight-cell NT embryos were higher than in fertilized embryos (**Figure 4C**), suggesting that those genes heavily marked by H3K9me3 modification likely affect the development potential of NT embryos.

GO analysis revealed that the genes associated with the higher H3K27me3 peaks in four-cell NT embryos affected pathways for dendritic development, synaptic signaling, and regulation of neuron projection (**Figure 4D**). Disruption of these pathways, which are critical for neural development and function, could adversely affect neural differentiation pathways in cloned embryos. In contrast, the genes associated with the higher H3K9me3 peaks in eight-cell NT embryos affect cellular component organization, developmental growth involved in morphogenesis, and appendage morphogenesis (**Figure 4E**).

Discussion

The efficiency of animal cloning is typically low because of limitations in developmental reprogramming in the cloned embryo. Epigenetic barriers to NT reprogramming, including incomplete or defective methylation of H3K9me3 [6], H3K4me3 [46], H3K27me3 [8, 47], H4K20me3 [9], inactivation of the X chromosome [12], and methylation of DNA [11], limit NT reprogramming and cloning success in mouse, bovine, goat, and pig species, but there are few studies on epigenetic barriers in rabbit NT reprogramming [4].

Here, we characterized the dynamic patterns of H3K9me3 and H3K27me3 in preimplantation NT rabbit embryos (one-cell, two-cell, four-cell, eight-cell, morula, and blastocyst). H3K9me3 in rabbit zygotes was associated with pericentric nucleolar structures in polar bodies and maternal but not paternal pronuclei (**Figure 1A**), whereas previous reports indicated that the paternal H3K9me3 pattern was established gradually during pronucleus (PN) development in mice and pigs [48]. Therefore, the H3K9me3 modification was delayed in the paternal pronucleus, indicating an asymmetric pattern of H3K9me3 in parental pronuclei [49]. We also found an asymmetric pattern of H3K9me3 in the parental pronuclei of rabbit zygotes. When a sperm penetrates the zona pellucida and enters the cytoplasm of an oocyte, the nucleus initiates paternal genome reprogramming through protamine phosphorylation, which is followed by a large-scale replacement of protamine by histones [48]. The

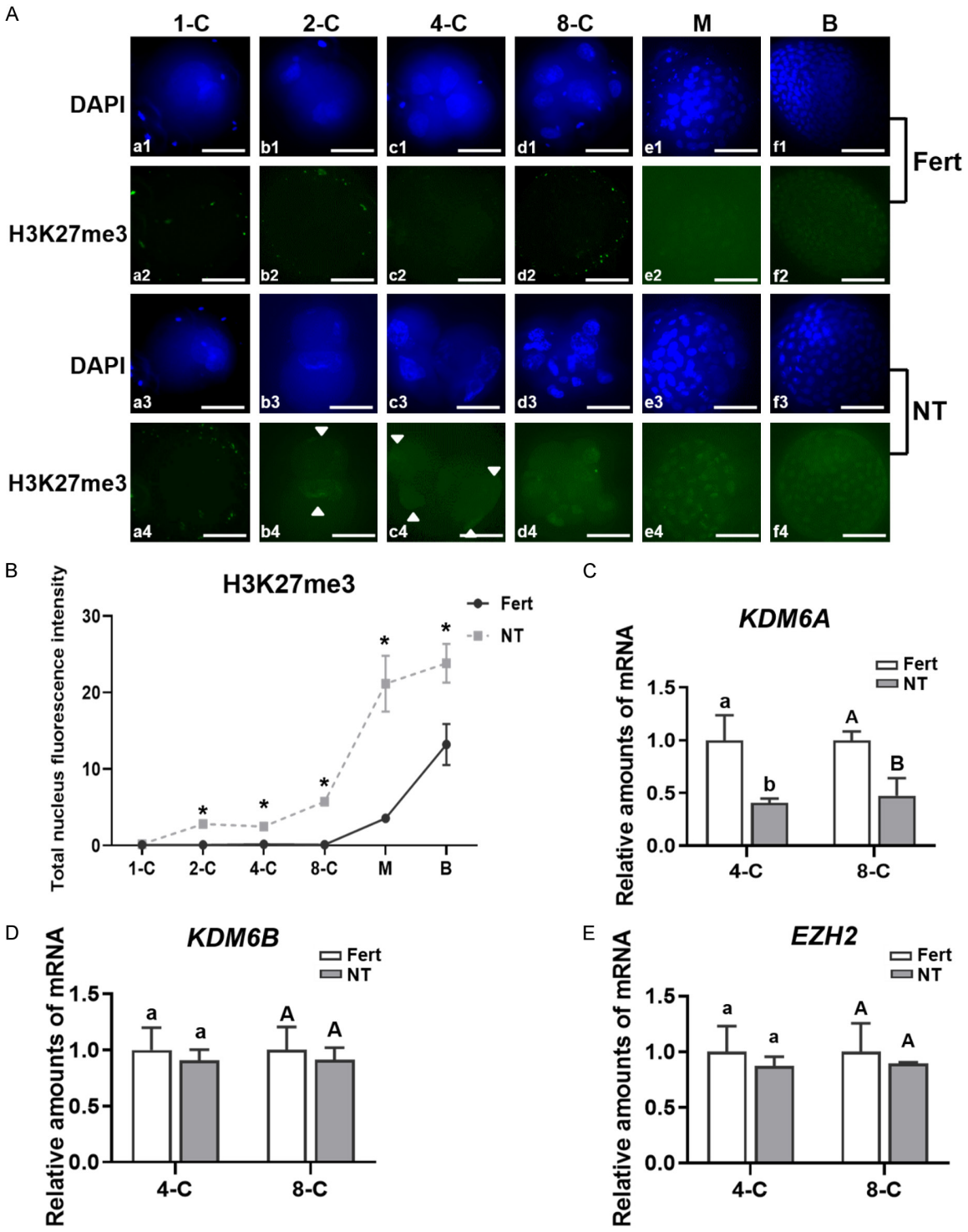

Figure 3. Patterns of H3K27me3 and expression of methyltransferase and demethylase RNA in fertilized and NT rabbit embryos. (A) H3K27me3 immunofluorescence staining of preimplantation fertilized and NT rabbit embryos. Arrowheads indicate a weak H3K9me3 signal. The H3K27me3 staining of fertilized embryos starts at the morula stage, whereas in NT embryos, it starts at the two-cell phase. Scale bar = 70 μm. (B) The H3K27me3 immunofluorescence intensity in two-cell, four-cell, eight-cell, and morula NT embryos was significantly higher than in fertilized embryos. *, $P < 0.05$. RNA expression levels of demethylase (C) *KDM6A,* (D) demethylase *KDM6B,* and (E) HMT *EZH2* in four-cell and eight-cell NT and fertilized embryos. Different lower-case letters (a, b) and upper-case letters (A, B) for four-cell and eight-cell embryos, respectively, in (C) indicate $P < 0.05$. There was no significant difference in *KDM6B* or *EZH2* RNA expression between NT and fertilized embryos. Experiments were done in triplicate with 123 fertilized and 112 NT embryos for immunofluorescence staining.

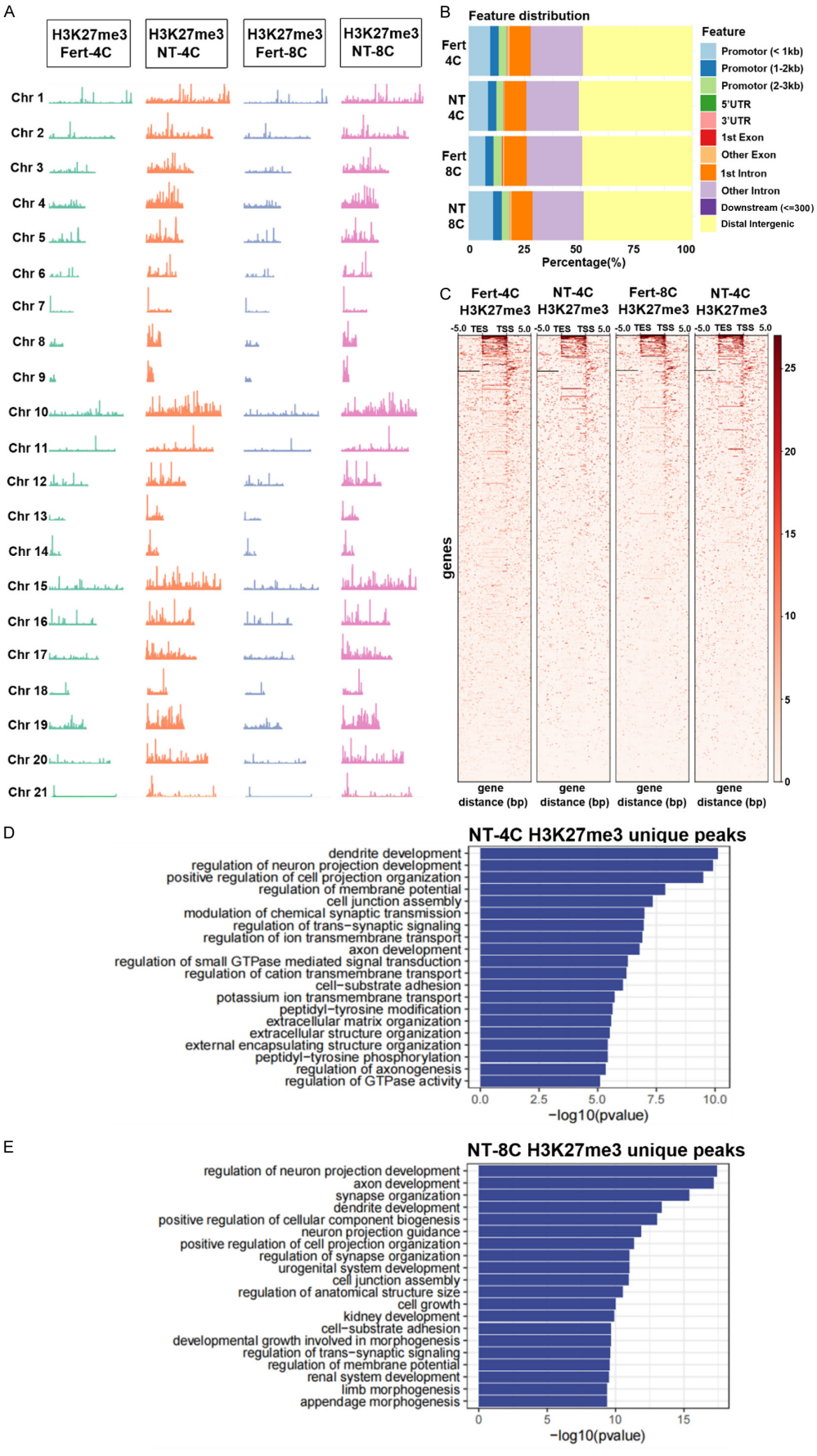
A
H3K27me3 Fert-4C
H3K27me3 NT-4C
H3K27me3 Fert-8C
H3K27me3 NT-8C
Chr 1
Chr 2
Chr 3
Chr 4
Chr 5
Chr 6
Chr 7
Chr 8
Chr 9
Chr 10
Chr 11
Chr 12
Chr 13
Chr 14
Chr 15
Chr 16
Chr 17
Chr 18
Chr 19
Chr 20
Chr 21
B
Feature distribution
Fert 4C
NT 4C
Fert 8C
NT 8C
0
25
50
75
100
Percentage(%)
Feature
Promotor (< 1kb)
Promotor (1-2kb)
Promotor (2-3kb)
5'UTR
3'UTR
1st Exon
Other Exon
1st Intron
Other Intron
Downstream (<=300)
Distal Intergenic
C
Fert-4C H3K27me3
NT-4C H3K27me3
Fert-8C H3K27me3
NT-4C H3K27me3
-5.0 TES TSS 5.0
genes
gene distance (bp)
25
20
15
10
5
0
D
NT-4C H3K27me3 unique peaks
dendrite development
regulation of neuron projection development
positive regulation of cell projection organization
regulation of membrane potential
cell junction assembly
modulation of chemical synaptic transmission
regulation of trans-synaptic signaling
regulation of ion transmembrane transport
axon development
regulation of small GTPase mediated signal transduction
regulation of cation transmembrane transport
cell-substrate adhesion
potassium ion transmembrane transport
peptidyl-tyrosine modification
extracellular matrix organization
extracellular structure organization
external encapsulating structure organization
peptidyl-tyrosine phosphorylation
regulation of axonogenesis
regulation of GTPase activity
0.0
2.5
5.0
7.5
10.0
-log10(pvalue)
E
NT-8C H3K27me3 unique peaks
regulation of neuron projection development
axon development
synapse organization
dendrite development
positive regulation of cellular component biogenesis
neuron projection guidance
positive regulation of cell projection organization
regulation of synapse organization
urogenital system development
cell junction assembly
regulation of anatomical structure size
cell growth
kidney development
cell-substrate adhesion
developmental growth involved in morphogenesis
regulation of trans-synaptic signaling
regulation of membrane potential
renal system development
limb morphogenesis
appendage morphogenesis
0
5
10
15
-log10(pvalue)

Figure 4. Global CUT and Tag analysis of H3K27me3 dynamics in NT and fertilized embryos. (A) Distribution of H3K27me3 binding sites across Chr 1-21 in four-cell and eight-cell fertilized and NT embryos. Each row represents a chromosome, and each colored line represents the signal intensity of the chromatin H3K27me3 modification. (B) The stacked bar chart illustrates the distribution of H3K27me3 CUT and Tag peaks on genomic features for four-cell and eight-cell NT vs. fertilized embryos. (C) A heatmap of H3K27me3 peaks from four-cell and eight-cell NT vs. fertilized embryos showing increased H3K27me3 peaks from the TSS to the TES in eight-cell NT vs. fertilized embryos. A darker red color indicates higher expression levels. (D and E) The GO analysis of the H3K27me3 unique peaks in which NT embryos bound more H3K27me3 than fertilized embryos, identified primarily genes that affect development. The x-axis, the -log10 (*P*-value), indicates the significance of the enrichment for each GO term. Experiments were done in triplicate with 15 four-cell and 9 eight-cell embryos each for fertilized and NT embryos.

delay in H3K9me3 modification in the paternal pronucleus is due to the time required for methyltransferases to convert mono-methylation to di- and tri-methylation on the newly synthesized histone H3.

H3K9me3 affects the accessibility and configuration of chromatin by preventing the binding of transcription factors, thereby inhibiting transcription [50, 51]. Aberrant patterns of H3K9me3, which are a major epigenetic barrier to the developmental competence of mouse NT embryos [6], are present in various animal species [3], including goat [52], bovine [25], and pig [26]. The increase in H3K9me3 in rabbit NT embryos vs. fertilized embryos from the one-cell to the blastocyst stages (**Figure 1**) is consistent with the data from cloned pig [26], goat [52], and bovine embryos [25]. Qin et al reported a significantly higher level of H3K9me3 in rabbit NT 8-cell embryos compared to fertilized embryos, which aligns with our findings (Qin et al, 2021). However, their study did not extend the comparison of H3K9me3 levels between NT and fertilized embryos at subsequent preimplantation stages [18]. Furthermore, Qu et al demonstrated that paternal (sperm-borne) small RNAs, specifically miR-34c and miR-125b, target and downregulate SUV39h1 [18]. Thereby reducing the levels of H3K9me3 and enhancing the developmental competence of rabbit NT embryos [17]. Dynamic changes in H3K9me3 modification patterns are controlled by methyltransferases SUV39H1/2 and demethylases in the KDM4 family [52]; however, the KDM enzymes vary by species. Here, we found no significant difference in the expression of *SUV39H1/2* and *KDM4B* between NT and fertilized embryos (**Figure 1D-F**), but there was a decrease in *KDM3B* expression in the four-cell and eight-cell stage NT embryos, which is inconsistent with the results for *KDM4B* and *KDM4D* in mouse and goat [6, 52], *KDM4E* in bovine species [25], and *KDM4A* in pig [26]. Overexpression of KDM4B, KDM4D, and KDM4E or inhibition of SUV39H1 downregulates H3K9me3 and greatly improves the reprogramming efficiency of NT embryos in many species [9]. Our data suggest that KDM3B is an epigenetic regulator during rabbit embryonic development that is defective for NT reprogramming. Thus, future research should determine whether *KDM3B* overexpression in NT one-cell embryos improves the cloning efficiency in rabbits.

H3K27me3, which represses transcription during early embryonic development, is involved in silencing the inactive X chromosome [12]. Here, we did not detect H3K27me3 until the morula stage in rabbit fertilized embryos [30], which is different from mouse [7], pig [53] and bovine species [8] in which H3K27me3 maintains a relatively high modification level during the process of cleavage but decreases dramatically after 8-cells, a process considered essential for normal embryonic genome activation. Our results indicate that H3K27me3 in the heterochromatin of fertilized preimplantation rabbit embryos may contribute to the remodeling and maintenance of the embryonic nuclear heterochromatin architecture. However, the higher H3K27me3 levels in NT embryos compared with fertilized embryos (**Figure 3B**) suggest that H3K27me3 was not reprogrammed normally in rabbit NT embryos, thereby repressing gene expression and the development of cloned rabbit embryos [53].

Histone demethylases KDM6A and KDM6B demethylate H3K27me3, whereas methylase EZH2 is antagonistic to KDM6A, maintaining H3K27me3 homeostasis during preimplantation embryo development. Here, we found that the expression of *KDM6A* decreased at the four-cell and eight-cell stages of NT rabbit embryos (**Figure 3**), which led to a high level of H3K27me3, consistent with the results in

mouse, pig, and bovine cloned embryos [7, 8, 29, 54]. Overexpression of KDM6A, which reduces H3K27me3, improves the development of mouse [54] and bovine NT embryos [8]. Similarly, the methyltransferase inhibitor GSK-126, which reduces H3K27me3, restores the global transcriptome in pig NT embryos [26]. As our data suggest that KDM6A is a key marker of rabbit NT reprogramming, overexpression of *KDM6A* may improve the efficiency of rabbit NT. It appears likely that the epigenetic barrier of H3K27me3 in rabbit NT reprogramming is evolutionarily conserved in other species.

Dramatic dynamic reprogramming of epigenetic landscapes during mammalian embryo development and the NT process [51, 55] resets epigenetic marks and changes chromatin structure and accessibility [51]. Incomplete or inaccurate H3K9me3 and H3K27me3 reprogramming inhibits NT embryo development [56]. CUT&Tag revealed aberrant enrichment of H3K9me3 peaks in chromosomes 4 and 17 of eight-cell NT embryos compared to the fertilized embryos (**Figure 2A**), whereas H3K27me3 peaks were enriched across all chromosomes in the four-cell and eight-cell stages in NT embryos (**Figure 4A**). Thus, the lack of reprogramming of H3K9me3 and H3K27me3 prevents ZGA and lineage commitment in NT rabbit embryos [50], and affects chromatin architecture reorganization and accessibility, supporting the important role of H3K9me3 and H3K27me3 in maintaining chromosome stability [50, 56]. We found enrichment of H3K9me3 and H3K27me3 at TSS sites in rabbit NT embryos (**Figures 2C** and **4C**), which results in chromatin compaction and reduces access by transcription factors and RNA polymerase II. This, in turn, inhibits the normal transcription of developmental genes (**Figures 2D** and **4D**) [57]. As the abnormal H3K9me3 and H3K27me3 modifications of NT embryos were enriched in the promoter regions and gene bodies of developmental genes (**Figures 2B** and **4B**), they primarily affect the expression of developmental genes [29, 50, 58]. Further, H3K9me3 and H3K27me3, as the hallmarks of heterochromatin, are mainly localized in the promoter regions of repressed genes and are essential for heterochromatin formation [23].

Conclusion

We found dynamic aberrant patterns of H3K9me3 and H3K27me3 modifications that serve as an epigenetic barrier to rabbit NT reprogramming. The hypermethylation of H3K9me3 and H3K27me3 is a result of a lack of demethylases KDM3B and KDM6A, respectively. The enrichment of H3K9me3 and H3K27me3 across the genome and specifically in the promoter regions of developmental genes inhibits their transcription, thereby blocking the normal development of NT embryos. Thus, our findings give insight into the roles of H3K9me3 and H3K27me3 in the regulation of gene expression and reprogramming cell plasticity in rabbit NT embryos and also suggest a strategy for improving the future success of cloning rabbits.

Acknowledgements

This study was supported by National Natural Science Foundation of China (NSFC) (Grant No. 32372877) to FD, and Postgraduate Research and Practice Innovation Program of Jiangsu Province (No. KYCX23_1742) to YG.

Disclosure of conflict of interest

None.

Address correspondence to: Fuliang Du and Zhihui Liu, Jiangsu Key Laboratory for Molecular and Medical Biotechnology, College of Life Sciences, Nanjing Normal University, #1 Wenyuan Road, Nanjing 210046, Jiangsu, PR China. E-mail: fuliangd@njnu.edu.cn (FLD); zhihuiliu@njnu.edu.cn (ZHL)

References

[1] Gurdon JB. The developmental capacity of nuclei taken from intestinal epithelium cells of feeding tadpoles. J Embryol Exp Morphol 1962; 10: 622-640.

[2] Wilmut I, Schnieke AE, McWhir J, Kind AJ and Campbell KH. Viable offspring derived from fetal and adult mammalian cells. Nature 1997; 385: 810-813.

[3] Matoba S and Zhang Y. Somatic cell nuclear transfer reprogramming: mechanisms and applications. Cell Stem Cell 2018; 23: 471-485.

[4] Cao W, Zhao J, Qu P and Liu E. Current progress and prospects in rabbit cloning. Cellular Reprogram 2022; 24: 63-70.

[5] Liu W, Liu X, Wang C, Gao Y, Gao R, Kou X, Zhao Y, Li J, Wu Y, Xiu W, Wang S, Yin J, Liu W, Cai T, Wang H, Zhang Y and Gao S. Identification of key factors conquering developmental arrest of somatic cell cloned embryos by combining embryo biopsy and single-cell sequencing. Cell discov 2016; 2: 16010.

[6] Matoba S, Liu Y, Lu F, Iwabuchi KA, Shen L, Inoue A and Zhang Y. Embryonic development following somatic cell nuclear transfer impeded by persisting histone methylation. Cell 2014; 159: 884-895.
[7] Yang L, Song L, Liu X, Bai L and Li G. KDM6A and KDM6B play contrasting roles in nuclear transfer embryos revealed by MERVL reporter system. EMBO Rep 2018; 19: e46240.
[8] Zhou C, Wang Y, Zhang J, Su J, An Q, Liu X, Zhang M, Wang Y, Liu J and Zhang Y. H3K27me3 is an epigenetic barrier while KDM6A overexpression improves nuclear reprogramming efficiency. FASEB J 2019; 33: 4638-4652.
[9] Liu Z, Wang W, Xia Y, Gao Y, Wang Z, Li M, Presicce GA, An L and Du F. Overcoming the H4K20me3 epigenetic barrier improves somatic cell nuclear transfer reprogramming efficiency in mice. Cell Prolif 2024; 57: e13519.
[10] Zhang S, Chen X, Wang F, An X, Tang B, Zhang X, Sun L and Li Z. Aberrant DNA methylation reprogramming in bovine SCNT preimplantation embryos. Sci Rep 2016; 6: 30345.
[11] Liu X, Wang Y, Gao Y, Su J, Zhang J, Xing X, Zhou C, Yao K, An Q and Zhang Y. H3K9 demethylase KDM4E is an epigenetic regulator for bovine embryonic development and a defective factor for nuclear reprogramming. Development 2018; 145: dev158261.
[12] Inoue K, Kohda T, Sugimoto M, Sado T, Ogonuki N, Matoba S, Shiura H, Ikeda R, Mochida K, Fujii T, Sawai K, Otte AP, Tian XC, Yang X, Ishino F, Abe K and Ogura A. Impeding Xist expression from the active X chromosome improves mouse somatic cell nuclear transfer. Science 2010; 330: 496-499.
[13] Honda A and Ogura A. Rabbit models for biomedical research revisited via genome editing approaches. J Reprod Dev 2017; 63: 435-438.
[14] Jia L, Ding B, Shen C, Luo S, Zhang Y, Zhou L, Ding R, Qu P and Liu E. Use of oocytes selected by brilliant cresyl blue staining enhances rabbit cloned embryo development in vitro. Zygote 2019; 27: 166-172.
[15] Chesne P, Adenot PG, Viglietta C, Baratte M, Boulanger L and Renard JP. Cloned rabbits produced by nuclear transfer from adult somatic cells. Nat Biotechnol 2002; 20: 366-369.
[16] Qin H, Qu P, Hu H, Cao W, Liu H, Zhang Y, Zhao J, Nazira F and Liu E. Sperm-borne small RNAs improve the developmental competence of pre-implantation cloned embryos in rabbit. Zygote 2021; 29: 331-336.
[17] Qu P, Cao W, Zhang Y, Qi J, Meng B, Liu S, Zhuang Y, Duan C and Liu E. Sperm-borne proteins improve rabbit cloning efficiency via regulating embryonic cleavage and epigenetics. Proteomics 2022; 22: e2200020.
[18] Qu P, Shen C, Du Y, Qin H, Luo S, Fu S, Dong Y, Guo S, Hu F, Xue Y and Liu E. Melatonin protects rabbit Somatic Cell Nuclear Transfer (SCNT) embryos from electrofusion damage. Sci Rep 2020; 10: 2186.
[19] Du F, Xu J, Zhang J, Gao S, Carter MG, He C, Sung LY, Chaubal S, Fissore RA, Tian XC, Yang X and Chen YE. Beneficial effect of young oocytes for rabbit somatic cell nuclear transfer. Cloning Stem Cells 2009; 11: 131-140.
[20] Sung LY, Chen CH, Xu J, Lin TA, Su HY, Chang WF, Liu CC, Sung YS, Cheng WT, Zhang J, Tian XC, Ju JC, Chen YE, Wu SC and Du F. Follicular oocytes better support development in rabbit cloning than oviductal oocytes. Cell Reprogram 2011; 13: 503-512.
[21] Chen C, Du F, Xu J, Chang WF, Liu CC, Su HY, Lin TA, Ju JC, Cheng WT, Wu SC, Chen YE and Sung LY. Synergistic effect of trichostatin A and scriptaid on the development of cloned rabbit embryos. Theriogenology 2013; 79: 1284-1293.
[22] Lachner M and Jenuwein T. The many faces of histone lysine methylation. Curr Opin Cell Biol 2002; 14: 286-298.
[23] Boland MJ, Nazor KL and Loring JF. Epigenetic regulation of pluripotency and differentiation. Circ Res 2014; 115: 311-324.
[24] Chung YG, Matoba S, Liu Y, Eum JH, Lu F, Jiang W, Lee JE, Sepilian V, Cha KY, Lee DR and Zhang Y. Histone demethylase expression enhances human somatic cell nuclear transfer efficiency and promotes derivation of pluripotent stem cells. Cell Stem Cell 2015; 17: 758-766.
[25] Liu X, Wang Y, Gao Y, Su J, Zhang J, Xing X, Zhou C, Yao K, An Q and Zhang Y. H3K9 demethylase KDM4E is an epigenetic regulator for bovine embryonic development and a defective factor for nuclear reprogramming. Development 2018; 145: dev158261.
[26] Weng XG, Cai MM, Zhang YT, Liu Y, Liu C and Liu ZH. Improvement in the in vitro development of cloned pig embryos after kdm4a overexpression and an H3K9me3 methyltransferase inhibitor treatment. Theriogenology 2020; 146: 162-170.
[27] Cao R and Zhang Y. The functions of E(Z)/EZH2-mediated methylation of lysine 27 in histone H3. Current Curr Opin Genet Dev 2004; 14: 155-164.
[28] Shpargel KB, Starmer J, Yee D, Pohlers M and Magnuson T. KDM6 demethylase independent loss of histone H3 lysine 27 trimethylation during early embryonic development. PLoS genet 2014; 10: e1004507.
[29] Liu X, Chen L, Wang T, Zhou J, Li Z, Bu G, Zhang J, Yin S, Wu D, Dou C, Xu T, He H, Zhu W, Yu L, Liu Z, Zhang X, Chen ZX and Miao YL. TDG is a

pig-specific epigenetic regulator with insensitivity to H3K9 and H3K27 demethylation in nuclear transfer embryos. Stem Cell Rep 2021; 16: 2674-2689.
[30] Liu J, An L, Wang J, Liu Z, Dai Y, Liu Y, Yang L and Du F. Dynamic patterns of H3K4me3, H3K27me3, and Nanog during rabbit embryo development. Am J Transl Res 2019; 11: 430-441.
[31] Kaya-Okur HS, Wu SJ, Codomo CA, Pledger ES, Bryson TD, Henikoff JG, Ahmad K and Henikoff S. CUT&Tag for efficient epigenomic profiling of small samples and single cells. Nat commun 2019; 10: 1930.
[32] Langmead B and Salzberg SL. Fast gapped-read alignment with Bowtie 2. Nature Methods 2012; 9: 357-359.
[33] Ton MN, Keitley D, Theeuwes B, Guibentif C, Ahnfelt-Ronne J, Andreassen TK, Calero-Nieto FJ, Imaz-Rosshandler I, Pijuan-Sala B, Nichols J, Benito-Gutierrez E, Marioni JC and Gottgens B. An atlas of rabbit development as a model for single-cell comparative genomics. Nat Cell Biol 2023; 25: 1061-1072.
[34] Tarasov A, Vilella AJ, Cuppen E, Nijman IJ and Prins P. Sambamba: fast processing of NGS alignment formats. Bioinformatics 2015; 31: 2032-2034.
[35] Li H, Handsaker B, Wysoker A, Fennell T, Ruan J, Homer N, Marth G, Abecasis G, Durbin R; 1000 Genome Project Data Processing Subgroup. The sequence alignment/map format and SAMtools. Bioinformatics 2009; 25: 2078-2079.
[36] Zhang Y, Liu T, Meyer CA, Eeckhoute J, Johnson DS, Bernstein BE, Nusbaum C, Myers RM, Brown M, Li W and Liu XS. Model-based analysis of ChIP-Seq (MACS). Genome Biol 2008; 9: R137.
[37] Li Q, Brown J, Huang H and Bickel P. Measuring reproducibility of high-throughput experiments. The The Ann Appl Stat 2011; 5: 1752-1779.
[38] Ramírez F, Ryan DP, Grüning B, Bhardwaj V, Kilpert F, Richter AS, Heyne S, Dündar F and Manke T. deepTools2: a next generation web server for deep-sequencing data analysis. Nucleic Acids Res 2016; 44: W160-W165.
[39] Yu G, Wang LG and He QY. ChIPseeker: an R/Bioconductor package for ChIP peak annotation, comparison and visualization. Bioinformatics 2015; 31: 2382-2383.
[40] Wang Q, Li M, Wu T, Zhan L, Li L, Chen M, Xie W, Xie Z, Hu E, Xu S and Yu G. Exploring epigenomic datasets by chipseeker. Curr Protoc 2022; 2: e585.
[41] Wu T, Hu E, Xu S, Chen M, Guo P, Dai Z, Feng T, Zhou L, Tang W, Zhan L, Fu X, Liu S, Bo X and Yu G. clusterProfiler 4.0: a universal enrichment tool for interpreting omics data. Innovation (Camb) 2021; 2: 100141.
[42] Wang C, Wang J, Song F, Liu H, Sun L, Wei X, Zheng T, Qian H, Li X, Zhang W, Tang X and Liu P. Upregulation of histone H3 caused by CRYAA may contribute to the development of age-related cataract. Biocell 2023; 47: 143-154.
[43] Wang D, Shi Y, Wang Z, Zhang J, Wang L, Ma H, Shi S, Lian X, Huang H, Wang X and Lian C. Meiotic nuclear divisions 1 suppresses the proliferation and invasion of pancreatic cancer cells via regulating H2A.X variant histone. Biocell 2024; 48: 111-122.
[44] Chen T, Chen X, Zhang S, Zhu J, Tang B, Wang A, Dong L, Zhang Z, Yu C, Sun Y, Chi L, Chen H, Zhai S, Sun Y, Lan L, Zhang X, Xiao J, Bao Y, Wang Y, Zhang Z and Zhao W. The genome sequence archive family: toward explosive data growth and diverse data types. Genomics Proteomics Bioinformatics 2021; 19: 578-583.
[45] CNCB-NGDC Members and Partners. Database resources of the national genomics data center, china national center for bioinformation in 2022. Nucleic Acids Res 2022; 50: D27-D38.
[46] Liu X, Wang C, Liu W, Li J, Li C, Kou X, Chen J, Zhao Y, Gao H, Wang H, Zhang Y, Gao Y and Gao S. Distinct features of H3K4me3 and H3K27me3 chromatin domains in pre-implantation embryos. Nature 2016; 537: 558-562.
[47] Matoba S, Wang H, Jiang L, Lu F, Iwabuchi KA, Wu X, Inoue K, Yang L, Press W, Lee JT, Ogura A, Shen L and Zhang Y. Loss of H3K27me3 imprinting in somatic cell nuclear transfer embryos disrupts post-implantation development. Cell Stem Cell 2018; 23: 343-354, e5.
[48] Liu Z, Cui J, Wang W, Li M, Wang Z, Presicce GA, Tian XC, An L and Du F. Dynamic and aberrant patterns of H3K4me3, H3K9me3, and H3K27me3 during early zygotic genome activation in cloned mouse embryos. Zygote 2022; 30: 903-909.
[49] Lepikhov K, Wossidlo M, Arand J and Walter J. DNA methylation reprogramming and DNA repair in the mouse zygote. Int J Dev Biol 2010; 54: 1565-1574.
[50] Xu R, Zhu Q, Zhao Y, Chen M, Yang L, Shen S, Yang G, Shi Z, Zhang X, Shi Q, Kou X, Zhao Y, Wang H, Jiang C, Li C, Gao S and Liu X. Unreprogrammed H3K9me3 prevents minor zygotic genome activation and lineage commitment in SCNT embryos. Nat commun 2023; 14: 4807.
[51] Du Z, Zhang K and Xie W. Epigenetic reprogramming in early animal development. Cold Spring Harb Perspect Biol 2022; 14: a039677.
[52] Deng M, Liu Z, Chen B, Wan Y, Yang H, Zhang Y, Cai Y, Zhou J and Wang F. Aberrant DNA and histone methylation during zygotic genome activation in goat cloned embryos. Theriogenology 2020; 148: 27-36.

[53] Xie B, Zhang H, Wei R, Li Q, Weng X, Kong Q and Liu Z. Histone H3 lysine 27 trimethylation acts as an epigenetic barrier in porcine nuclear reprogramming. Reproduction 2016; 151: 9-16.
[54] Bai GY, Song SH, Zhang YW, Huang X, Huang XW, Sun RZ and Lei L. Kdm6a overexpression improves the development of cloned mouse embryos. Zygote 2018; 26: 24-32.
[55] Wang C, Liu X, Gao Y, Yang L, Li C, Liu W, Chen C, Kou X, Zhao Y, Chen J, Wang Y, Le R, Wang H, Duan T, Zhang Y and Gao S. Reprogramming of H3K9me3-dependent heterochromatin during mammalian embryo development. Nat Cell Biol 2018; 20: 620-631.
[56] Fukushima HS, Takeda H and Nakamura R. Incomplete erasure of histone marks during epigenetic reprogramming in medaka early development. Genome Res 2023; 33: 572-586.
[57] Zou Z, Wang Q, Wu X, Schultz RM and Xie W. Kick-starting the zygotic genome: licensors, specifiers, and beyond. EMBO Rep 2024; 25: 4113-4130.
[58] Wang LY, Li ZK, Wang LB, Liu C, Sun XH, Feng GH, Wang JQ, Li YF, Qiao LY, Nie H, Jiang LY, Sun H, Xie YL, Ma SN, Wan HF, Lu FL, Li W and Zhou Q. Overcoming intrinsic H3K27me3 imprinting barriers improves post-implantation development after somatic cell nuclear transfer. Cell Stem Cell 2020; 27: 315-325.